Atmósfera 40, 189-207 (2026)
https://doi.org/10.20937/ATM.53539

Changes in the Caribbean Low-Level Jet in the recent climate period and CMIP6 climate change scenarios

David GARZÓN-CASAS and José Franlyn RUIZ-MURCIA

Universidad Nacional de Colombia, Bogotá, 111321, Bogotá, Colombia.
*Corresponding author; email: dgarzonc@unal.edu.co

Received: September 19, 2025; Accepted: February 12, 2026

RESUMEN

La Corriente de Chorro de Bajo Nivel del Caribe (CLLJ, por su sigla en inglés) es un componente atmosférico crucial que controla la variabilidad climática y el transporte de humedad en la región del Caribe. Este estudio analiza las tendencias históricas y las proyecciones futuras del CLLJ utilizando datos observacionales, productos de reanálisis y modelos climáticos del Proyecto de Intercomparación de Modelos Acoplados Fase 6 (CMIP6). El análisis histórico (1981-2020) revela un debilitamiento del CLLJ, respaldado por tres de cuatro productos de reanálisis que muestran disminuciones de la velocidad del viento de –0.02 a –0.05 m s^{-1} y^{-1} a 925 hPa, consistente con las reducciones observadas en el gradiente de presión entre el Anticiclón Subtropical del Atlántico Norte (NASH) y el Sistema de Baja Presión de Panamá. La variabilidad natural multidecadal, incluyendo la Oscilación Multidecadal del Atlántico (AMO) y la Oscilación Decadal del Pacífico (PDO), probablemente ha contribuido a este debilitamiento. Los modelos CMIP6 muestran una habilidad limitada para reproducir las características históricas del CLLJ, ya que solo el 18% captura las tendencias de debilitamiento observadas y el 82% no alcanza un RMSE* < 1, lo que indica un desempeño inferior al de la climatología. Las proyecciones futuras (2015-2099) muestran una clara dependencia del escenario: el escenario de bajas emisiones (SSP1-2.6) mantiene las condiciones actuales, mientras que los escenarios de altas emisiones (SSP3-7.0 y SSP5-8.5) impulsan un fortalecimiento progresivo debido a gradientes de presión más intensos. Los cambios estacionales redistribuyen la intensidad del CLLJ, debilitando los máximos de invierno y fortaleciendo los mínimos de otoño, lo que podría eliminar la estructura bimodal actual en el contexto de emisiones altas. Estos hallazgos tienen implicaciones profundas para los recursos hídricos regionales y la energía renovable, por lo que requieren estrategias de gestión adaptativa que consideren las incertidumbres de las proyecciones.

ABSTRACT

The Caribbean Low-Level Jet (CLLJ) is a crucial atmospheric feature controlling climate variability and moisture transport in the Caribbean region. This study analyzes historical trends and future projections of the CLLJ using observational data, reanalysis products, and Coupled Model Intercomparison Project Phase 6 (CMIP6) climate models. Historical analysis (1981-2020) reveals CLLJ weakening, supported by three of the four reanalysis products showing wind-speed decreases of –0.02 to –0.05 m s^{-1} y^{-1} at 925 hPa, consistent with observed pressure-gradient reductions between the North Atlantic Subtropical High (NASH) and Panama Low. Natural multidecadal variability, including the Atlantic Multidecadal Oscillation (AMO) and Pacific Decadal Oscillation (PDO), likely contributed to this weakening. CMIP6 models demonstrate limited skill in reproducing historical CLLJ characteristics, with only 18% capturing observed weakening trends and 82% failing to achieve RMSE* < 1, indicating skill inferior to climatology. Future projections (2015-2099) show clear scenario dependence: the low emission scenario (SSP1-2.6) maintains current conditions while high emission scenarios (SSP3-7.0 and SSP5-8.5) drive progressive strengthening through enhanced pressure gradients. Seasonal changes redistribute CLLJ intensity, weakening winter maxima while strengthening autumn minima, potentially eliminating the current bimodal structure under high emissions. These findings have profound implications for regional water resources and renewable energy, requiring adaptive management strategies that account for projection uncertainties.

Keywords: Caribbean Low-Level Jet, CMIP6, climate projections, reanalysis, climate trends.

1. Introduction

The Caribbean Low-Level Jet (CLLJ) is a critical atmospheric feature that controls moisture transport, precipitation patterns, and wind energy resources across the Caribbean, Central America, and northwestern South America. Understanding its response to anthropogenic climate change has become increasingly urgent: global surface temperatures have risen 0.9-1.2 ºC above preindustrial levels (Chen et al., 2021; Gulev et al., 2021), inducing widespread circulation changes including Hadley Cell expansion at 0.1-0.5º latitude per decade (Gulev et al., 2021). Yet how these large-scale changes manifest in regional features like the CLLJ remains inadequately understood.

The CLLJ is a low-level atmospheric jet with its core at 925 hPa, extending zonally along 15º N between 80º and 70º W, with maximum wind speeds reaching 16 m s^{-1}, confined to heights below 600 hPa (Wang, 2007; Whyte et al., 2007; Muñoz et al., 2008). It exhibits pronounced bimodal seasonality with maxima during June-July and December-February, controlled by the meridional pressure gradient between the North Atlantic Subtropical High (NASH) and Panama Low-Pressure System (Poveda and Mesa, 1999; Amador, 2008). The jet serves as the primary moisture conveyor from the Caribbean Sea to Central America, transporting up to 10 mm day^{-1}, an order of magnitude larger than Pacific contributions (Durán-Quesada et al., 2017). During peak intensity, it modulates sea surface temperatures, enhances upwelling, and contributes to the midsummer drought through complex air-sea interactions (Herrera et al., 2015). On interannual-to-decadal timescales, El Niño-Southern Oscillation (ENSO), North Atlantic Oscillation (NAO), Atlantic Multidecadal Oscillation (AMO), and Pacific Decadal Oscillation (PDO) jointly modulate jet intensity (Giannini et al., 2001; Wang, 2007; Whyte et al., 2007; Bastidas-Salamanca and Rueda-Bayona, 2021; Cerón et al., 2021).

The climate model representation of the CLLJ has historically posed significant challenges. Martin and Schumacher (2011) demonstrated that CMIP3 models systematically failed to reproduce the observed CLLJ semiannual cycle, simulating uniform wind speeds between January and July rather than the characteristic July peak. This bias stemmed from inadequate representation of the NASH seasonal evolution, particularly its westward and southward expansion during boreal summer. These deficiencies reflect broader challenges in simulating tropical circulation features at typical CMIP resolutions (100-200 km), which inadequately resolve mesoscale topographic influences through Central American gaps and coastal mountain ranges. Whether CMIP6 models have addressed these fundamental simulation challenges remains an open question.

Previous modeling studies examining CLLJ response to anthropogenic forcing have yielded notably conflicting results across model generations and scenarios. Taylor et al. (2012) used the PRECIS regional model under A2 and B2 scenarios to project CLLJ intensification by the late 21st century, particularly during the traditional weakening season (August-October), with core jet strength increasing 7-8 m s^{-1} by 2071-2100 relative to 1961-1990. They linked this strengthening to persistent, strong low-level winds, which contribute to projected Caribbean drying through the extended rainy season. In contrast, Imbach et al. (2018) used the Eta Regional Climate Model driven by HadGEM2-ES under RCP4.5 and found that CLLJ winds at 925 hPa weaken throughout the year by mid-century (2021-2050), though they noted little overall climate change impact on the CLLJ and some strengthening in upper layers during boreal summer months.

Regional climate model studies have added further complexity to this picture. Vichot-Llano et al. (2022) employed a multiparameter ensemble of RegCM4 configurations with different cumulus parameterizations driven by the CMIP5 model

HadGEM2-ES and found consistent strengthening of the CLLJ during boreal summer months (0.2-3.8 m s^{-1} by the end of the century) and weakening during boreal winter months (0.6-1 m s^{-1}), with consensus across all ensemble members. Regional assessments project enhanced wind resources in the CLLJ region through the 21st century, driven primarily by wet-season strengthening linked to changes in atmospheric circulation. Under CMIP5 RCP8.5 scenarios, dry-season increases were limited to the southeastern Venezuelan coast (Costoya et al., 2019). Updated CMIP6 projections under SSP5-8.5 confirm these trends with greater spatial detail, revealing 30-40% wind power density increases during boreal summer in the CLLJ region, alongside significant gains (> 0.54% y^{-1}) along the Colombian-Venezuelan coastline, though with notable seasonal variability (Arregocés et al., 2025).

Most recently, Bustos and Torres (2023) evaluated 24 CMIP6 models for Caribbean wind simulation, with 10 models showing good skill in reproducing broad-scale Caribbean patterns and variability (1990-2014) based on six validation metrics. However, model skill was not validated specifically for CLLJ representation or for reproducing historical trends. Using a multi-model mean, they projected CLLJ strengthening of 0.16 ± 0.03 m s^{-1} per century (SSP2-4.5) and 0.45 ± 0.03 m s^{-1} per century (SSP5-8.5) for 2015-2100, with greatest intensification during the wet season.

While these studies reveal emerging patterns—particularly strengthening under high-emission scenarios and pronounced seasonal asymmetry—the magnitude and even the direction of projected changes remain uncertain. This uncertainty reflects not only differences in emission scenarios and model physics across CMIP generations, but critically, the absence of systematic validation of model skill in reproducing historical CLLJ characteristics. Most projection studies, including the recent CMIP6 assessment by Bustos and Torres (2023), evaluate model performance for broad Caribbean wind patterns but not specifically for CLLJ representation or historical trend reproduction. Without such validation, distinguishing genuine climate responses from systematic model biases remains challenging, undermining confidence in projected changes.

This study provides a comprehensive analysis of CLLJ changes using the latest CMIP6 model ensemble, addressing critical gaps in understanding historical trends and future projections. Specifically, the analysis: (1) reconciles conflicting evidence of historical CLLJ trends using multiple observational and reanalysis datasets; (2) evaluates CMIP6 model performance in simulating historical CLLJ characteristics, including their ability to reproduce observed trends; (3) projects future CLLJ changes under four SSP scenarios, examining seasonal variations; and (4) analyzes the underlying dynamical mechanisms driving these changes through surface pressure system variations in the NASH and Panama Low Pressure System.

2. Data and methods

2.1 Study area

Two analysis domains were defined (Fig. 1): (1) the CLLJ core region (12.5º-17.5º N, 80º-70º W) following Muñoz et al. (2008), and (2) a large-scale domain encompassing the Caribbean Sea, tropical North Atlantic, and Gulf of Mexico (2º S-50º N, 90º-2.5º W) to examine synoptic-scale controls on regional wind patterns and moisture transport pathways.

2.2 Observational and reanalysis data

2.2.1 In-situ observations

Radiosonde data from 37 stations were obtained from NOAA's Integrated Global Radiosonde Archive (IGRA-2), selected for > 60% data availability during 1991-2020. Two stations are particularly relevant for CLLJ analysis: Curaçao, located within the jet core area, and San Andrés, positioned at the jet's exit region. The remaining stations were used to assess synoptic patterns affecting the Caribbean. Additionally, 313 NOAA buoy stations with information from 2005 to 2024 and at least 15 years of records provided surface wind and pressure measurements (Fig. 1).

2.2.3 Reanalysis products

Five reanalysis datasets were analyzed for 1991-2020: ERA5 (0.25º × 0.25º), NCEP/DOE Reanalysis 2 (2.5º × 2.5º), 20th Century Reanalysis (1º × 1º), MERRA-2 (0.625º × 0.5º), and CCMP (0.25º × 0.25º). Variables included wind components and air pressure at 925 hPa and at the surface. ERA5 served as the primary reference for model validation due to its demonstrated skill in the region (Gil et al., 2021).

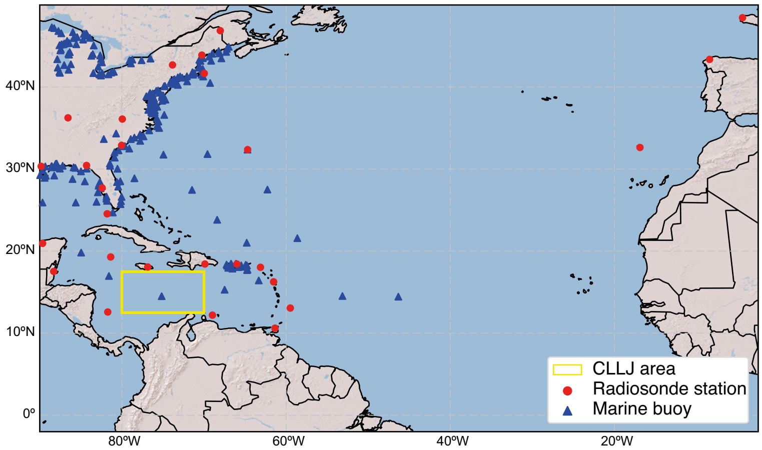

Fig. 1. Map of the study area showing the large-scale analysis domain encompassing the Caribbean Sea, tropical North Atlantic, and Gulf of Mexico. Red dots indicate radiosonde stations, and blue triangles show marine buoy locations used in the analysis. The yellow box delineates the CLLJ area.

2.3 CMIP6 climate models

A total of 34 CMIP6 models from 23 modeling institutions were analyzed for the historical period 1981-2014, with model availability varying by future scenario (2015-2099): 28 models for SSP1-2.6, 27 models for SSP2-4.5, 26 models for SSP3-7.0, and 29 models for SSP5-8.5 (Table S1 in the supplementary material). These four shared socioeconomic pathway (SSP) scenarios span radiative forcing levels from low emissions (SSP1-2.6: ~2.6 W m^{-2}) to high emissions (SSP5-8.5: ~8.5 W m^{-2}) by 2100, representing pathways from strong climate mitigation to fossil-fueled development (O'Neill et al., 2016).

All model data were obtained from the Copernicus Climate Data Store (CDS). Model selection prioritized data completeness for the required variables (monthly mean wind speed at 925 hPa and sea level pressure) and temporal coverage across both historical and projection periods. Model outputs were standardized to 1° × 1° resolution via bilinear interpolation to facilitate inter-model comparison.

For each model, the first available ensemble member was used, which was typically r1i1p1f1 but occasionally r1i1p1f2 or r1i1p1f3 depending on data availability in the CDS archive. Multi-model ensemble statistics were calculated using all available models for each scenario, with equal weighting across models.

2.4 Trend analysis and validation

Linear trends were calculated using least-squares regression, with confidence intervals estimated using the Newey-West method to account for autocorrelation and heteroscedasticity in climate time series. Trends were categorized as significantly positive, significantly negative, or non-significant based on the positions of the confidence interval bounds.

Model performance was evaluated using standardized metrics following Wadoux et al. (2022): mean error (ME), standard deviation of error (SDE), and root mean square error (RMSE*), visualized using solar diagrams. In these diagrams, ME* and SDE* are plotted on the x and y axes, respectively, while RMSE* is represented radially, with the three metrics related by $RMSE^2 = ME^2 + SDE^2$. The asterisk (*) indicates standardization by the observed standard deviation (σ), enabling multi-variable comparison. Models with RMSE* < 1 were considered skillful, as this threshold indicates better performance than using the climatological mean as a predictor, demonstrating the model's ability to capture not only mean values but also temporal variability.

3. Results

3.1 Historical trends in large-scale controls

Analysis of observational and reanalysis data for 1991-2020 revealed complex and sometimes contradictory trends in Caribbean wind patterns. Surface wind speeds from marine buoys showed significant negative trends in the central and western Caribbean Sea, with the station nearest to Colombian waters (NDBC 42058) recording –0.05 m s^{-1} y^{-1} (Fig. 2). However, CCMP satellite estimates for 1992-2023 indicated non-significant trends in the same region, highlighting observational uncertainties (Fig. 3).

At 925 hPa, radiosonde observations showed predominantly positive trends across the analysis domain (Fig. 4). The San Andrés station exhibited non-significant trends, while Curaçao, located within

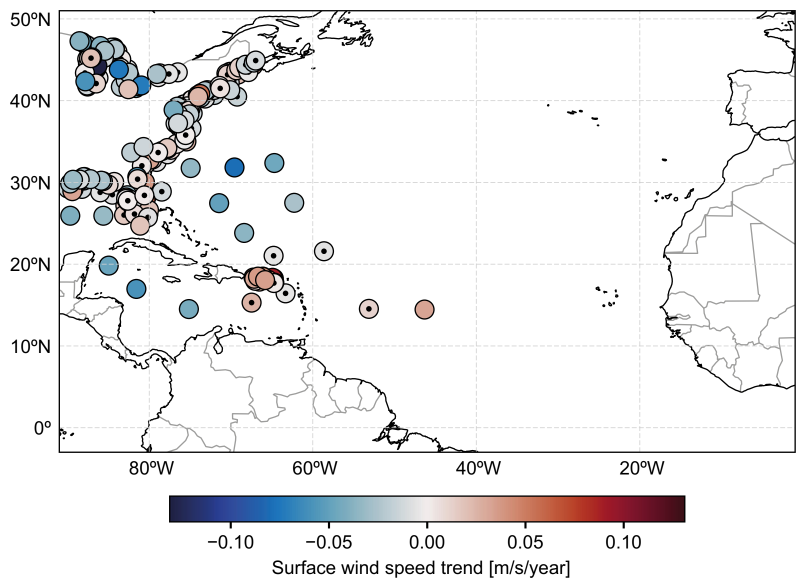

Fig. 2. Trend of surface wind speed recorded by marine buoys (2005-2024). Circle colors indicate trend magnitude (m s^{-1} y^{-1}) according to the color scale. Points indicate non-significant trends.

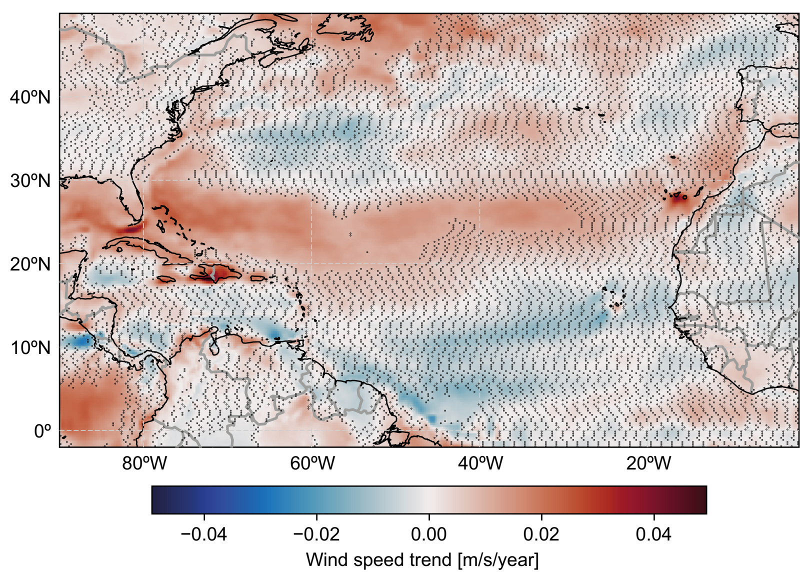

Fig. 3. Trend of surface wind speed estimated by CCMP (1992-2023). Points indicate non-significant trends.

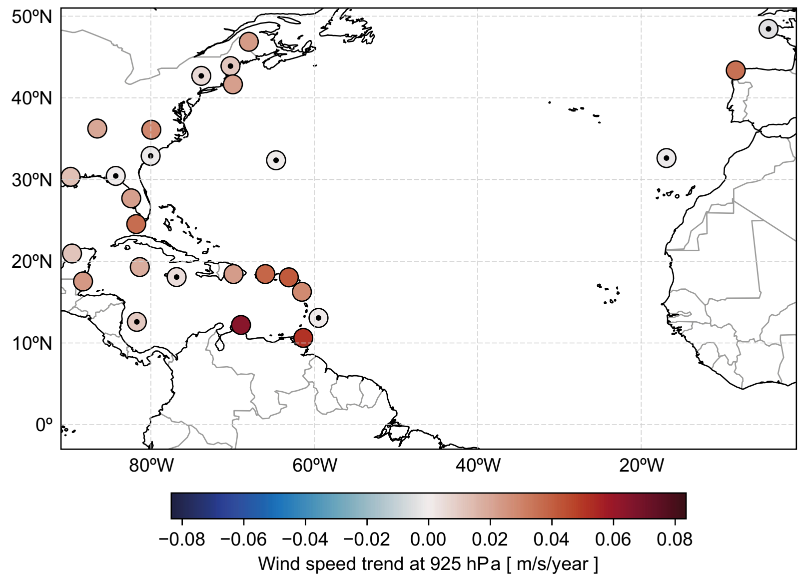

Fig. 4. Trend of wind speed at 925 hPa recorded by radiosondes (1981-2010). Points indicate non-significant trends.

the CLLJ influence zone, showed significant strengthening of +0.06 m s^{-1} y^{-1} concentrated at the jet core level. This vertical structure, with maximum trends at 925 hPa and decreasing values above and below, is characteristic of jet intensification (Fig. 5).

Reanalysis products displayed greater consistency but diverged from observations. ERA5, MERRA-2, and 20th Century Reanalysis showed significant weakening (–0.02 to –0.05 m s^{-1} y^{-1}) throughout most of the Caribbean basin at 925 hPa, with minimum

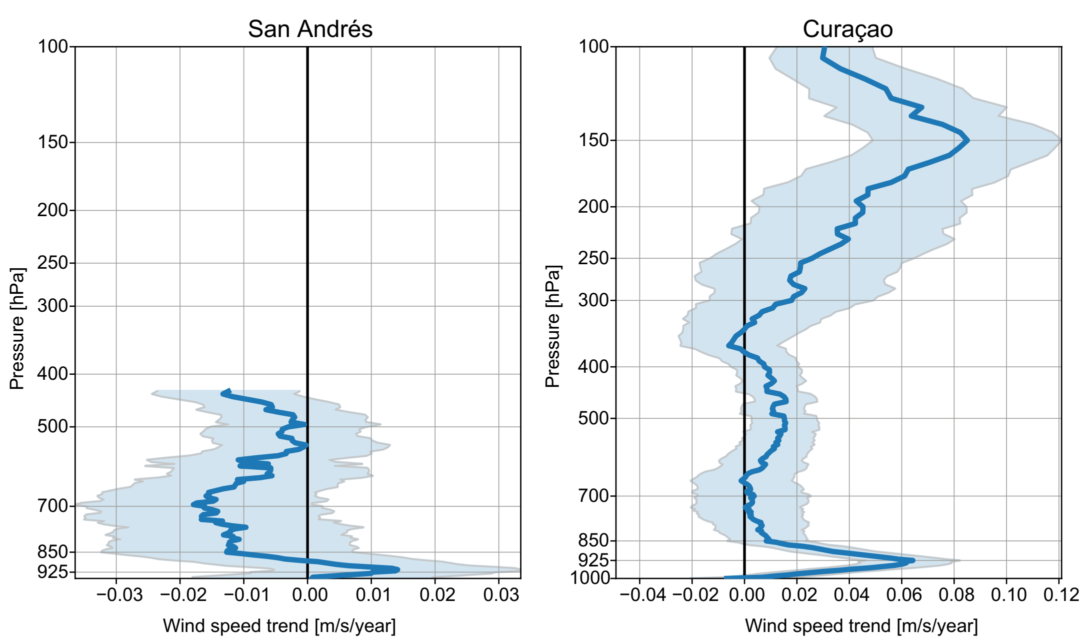

Fig. 5. Vertical profiles of wind speed trends recorded by radiosondes at San Andrés and Curaçao stations, showing trend magnitude with confidence intervals.

trends north and west of the Guajira Peninsula. Conversely, NCEP/DOE Reanalysis 2 indicated strengthening (0.02 m s^{-1} y^{-1}), aligning more closely with radiosonde observations (Fig. 6).

Surface pressure analysis provided mechanistic insights into wind trends. Buoy observations and all four reanalyses showed consistent patterns: significant pressure increases of approximately 0.01 hPa y^{-1} over Panama and the eastern tropical Pacific where the Panama Low typically resides, and pressure decreases (–0.04 to –0.05 hPa y^{-1}) in the NASH core region (Figs. 7 and 8). This reduced pressure gradient across the Caribbean basin is dynamically consistent with the wind weakening indicated by most reanalyses.

The historical weakening signal, though not unanimous across datasets, appears robust when considering multiple factors. Three of four reanalyses show consistent weakening patterns dynamically linked to observed reductions in the pressure gradient. The disagreement with radiosonde observations may reflect spatial sampling limitations, as only two stations directly sample the CLLJ region, compounded by technological and methodological changes in radiosonde wind estimation that may compromise the reliability of this observational source.

The 1991-2020 analysis period coincided with AMO warm-phase consolidation and PDO cold phase, a combination associated with CLLJ weakening, according to Cerón et al. (2021). Because these multidecadal oscillations modulate the basin-scale SST gradients that control CLLJ intensity on multiple timescales (Whyte et al., 2007; Cerón et al., 2021), this configuration provides independent support for the observed weakening trend, suggesting that the CLLJ likely experienced genuine weakening during recent decades driven by natural interdecadal variability rather than anthropogenic climate change signals.

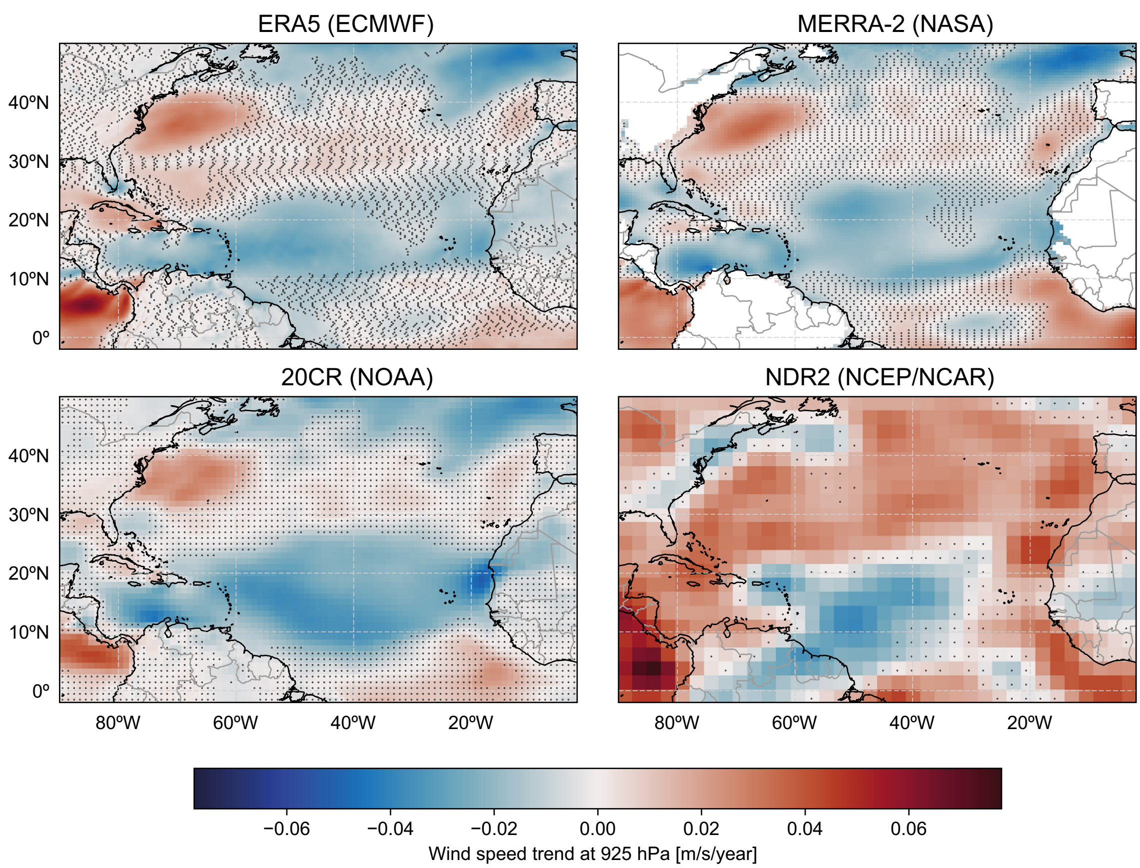

Fig. 6. Trend of wind speed at 925 hPa estimated by four reanalysis products (1991-2020). Points indicate non-significant trends.

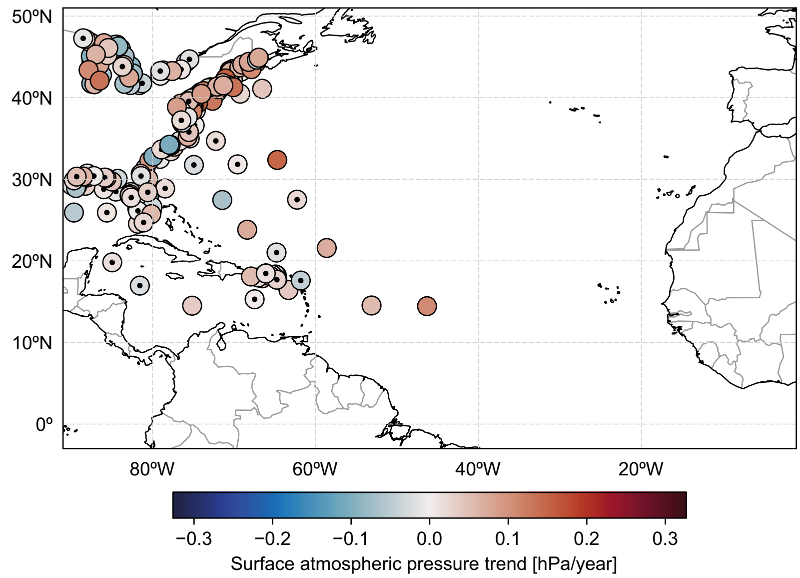

Fig. 7. Trend of surface atmospheric pressure recorded by marine buoys (2005-2024). Points indicate non-significant trends.

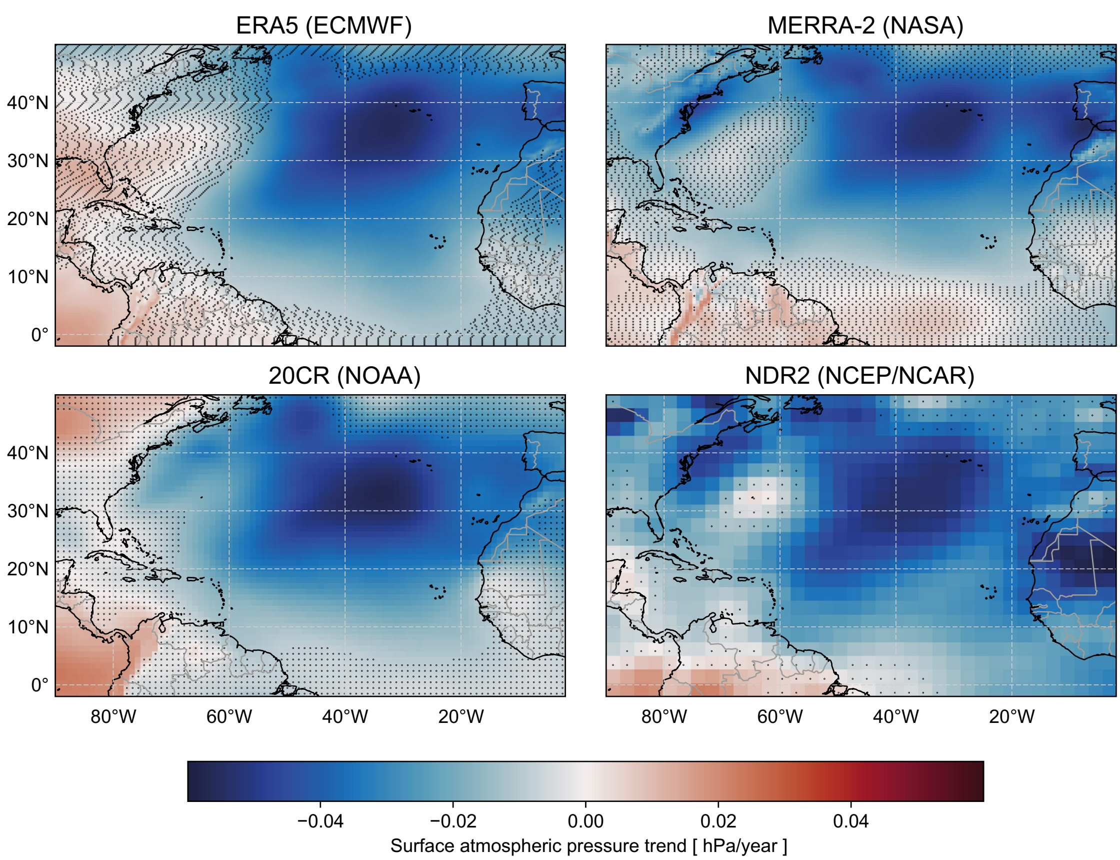

Fig. 8. Trend of surface atmospheric pressure estimated by four reanalysis products (1991-2020). Points indicate non-significant trends.

3.2 CLLJ changes in historical period

Spatial analysis of CLLJ trends (1981-2010) revealed substantial disagreement among reanalyses (Fig. 9). Within the jet core region, ERA5 showed 71% of area with negative trends and 29% non-significant; MERRA-2 and 20th Century Reanalysis showed even stronger weakening signals (91 and 100% negative areas, respectively). NCEP/DOE Reanalysis 2 contrasted sharply with 87% positive trend area.

CMIP6 historical simulations poorly reproduced observed CLLJ trends. Models were classified into three groups based on trend patterns: Group 1 (18% of models) with > 30% negative trend areas, Group 2 (71%) dominated by non-significant trends, and Group 3 (11%) with > 30% positive trends (Fig. 10). The predominance of Group 2 indicates most models failed to capture the weakening trend suggested by three of four reanalyses.

Validation against ERA5 revealed systematic deficiencies in CMIP6 CLLJ simulation. Only eight

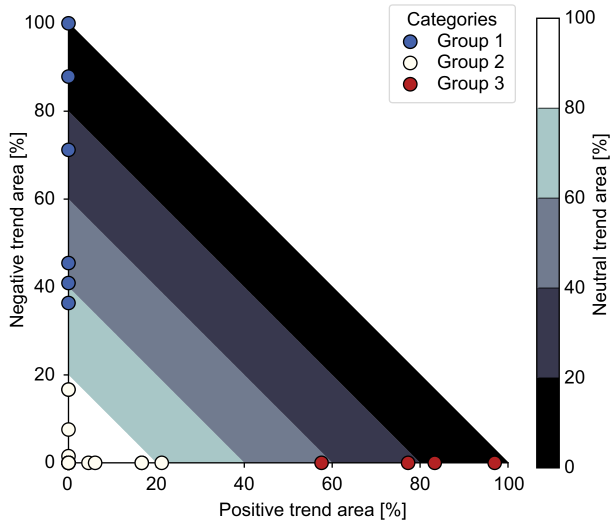

Fig. 10. Distribution diagram of area percentage for trend categories of wind speed at 925 hPa in the CLLJ area, modeled by 34 CMIP6 models during the historical period. Colors indicate model groups based on dominant trend patterns.

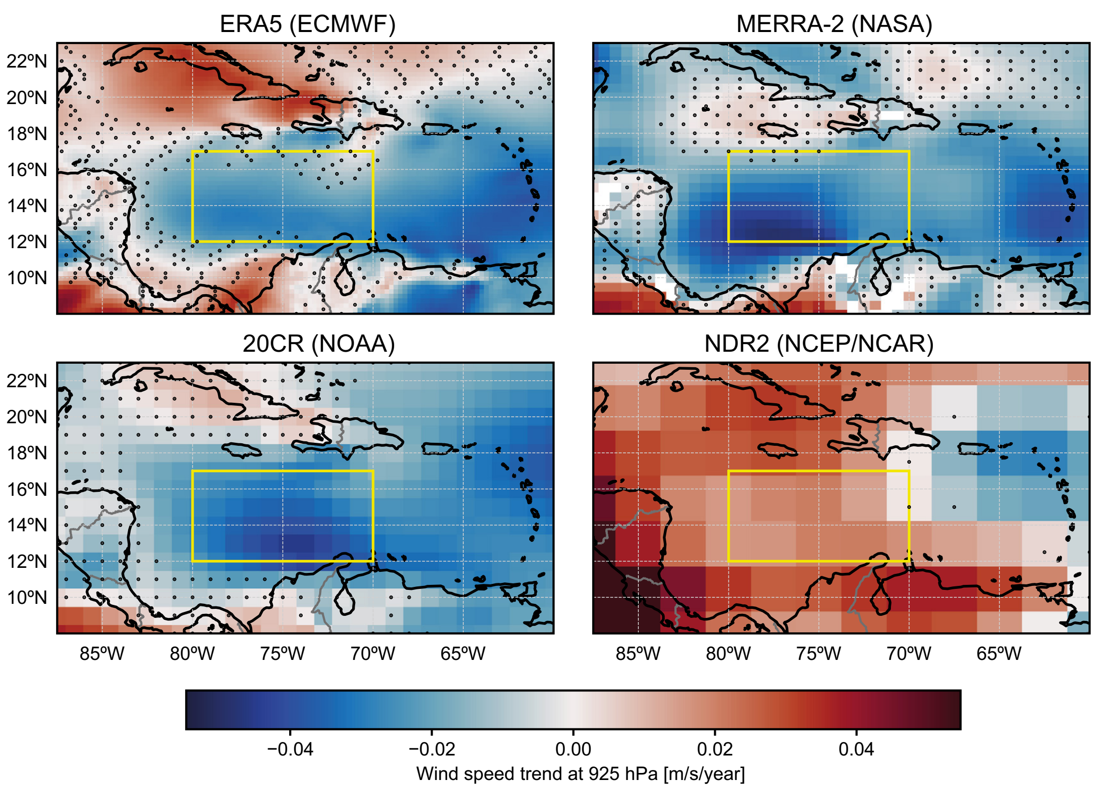

Fig. 9. Trend of wind speed at 925 hPa estimated by four reanalysis products (1981-2010). The yellow box indicates the CLLJ area. Points indicate non-significant trends.

of the 34 models achieved RMSE* < 1 (those models inside the unit circumference in the verification diagram, Fig. 11), indicating skill superior to climatological forecasts. The remaining 26 models showed high SDE* values with ME* scattered around zero, demonstrating an inability to reproduce jet variability rather than systematic bias. This poor performance continues a pattern identified in earlier CMIP generations, where models systematically failed to reproduce the CLLJ semiannual cycle and underestimated peak intensity (Martin and Schumacher, 2011).

The models' limited skill in reproducing historical CLLJ characteristics reflects broader challenges in simulating regional jets and their controlling mechanisms. Given that the CLLJ exhibits substantial multidecadal variability modulated by coupled ocean-atmosphere modes (Cerón et al., 2021), and these models exhibit well-documented deficiencies in representing PDO variability (Ma et al., 2023) and AMO characteristics (Robson et al., 2023), these circumstances likely contribute to their poor CLLJ simulation. These representation errors mean models may misattribute forced changes to natural variability or vice versa, introducing systematic errors into attribution of historical trends and undermining confidence in future projections.

Notably, previous CMIP6 projection studies have not systematically validated model skill in reproducing historical CLLJ trends before using these models for future projections. This validation gap is particularly problematic given the present results: with only 24% of models showing skill superior to climatology and 82% failing to capture observed weakening patterns, future projections from the full ensemble may reflect model biases as much as genuine climate responses.

3.3 CLLJ future projections

CMIP6 projections for 2015-2099 showed clear scenario-dependent CLLJ evolution (Fig. 12). Under SSP1-2.6, most models projected non-significant trends with limited spatial coherence. Higher

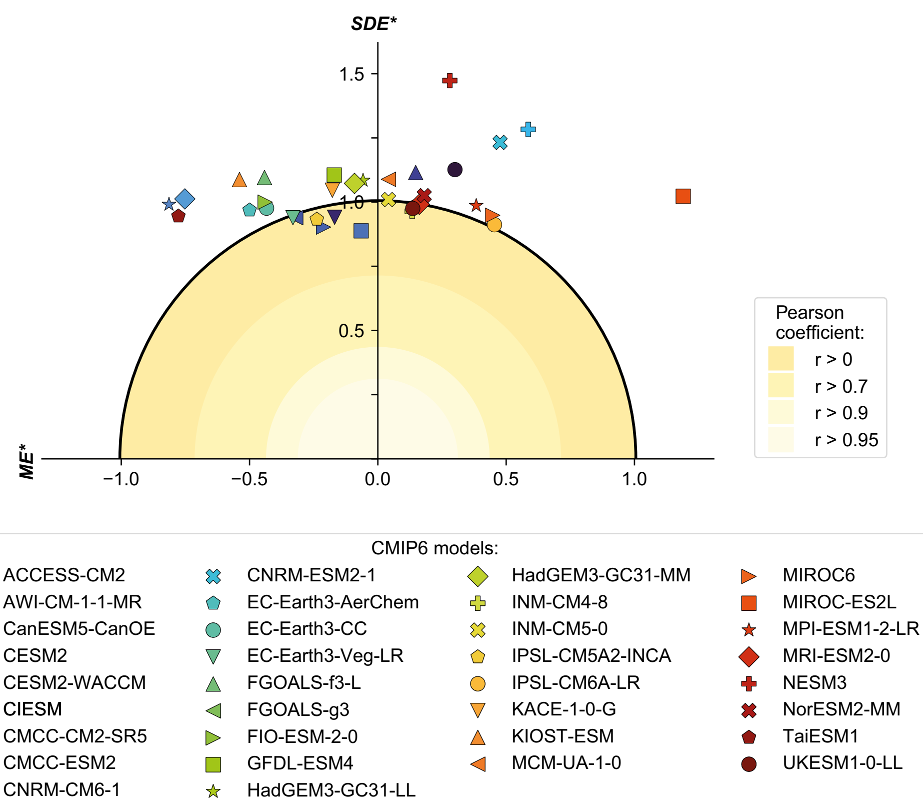

Fig. 11. Solar diagram for validation of mean wind speed simulations in the CLLJ area at 925 hPa from CMIP6 models during the historical period using ERA5 as reference.

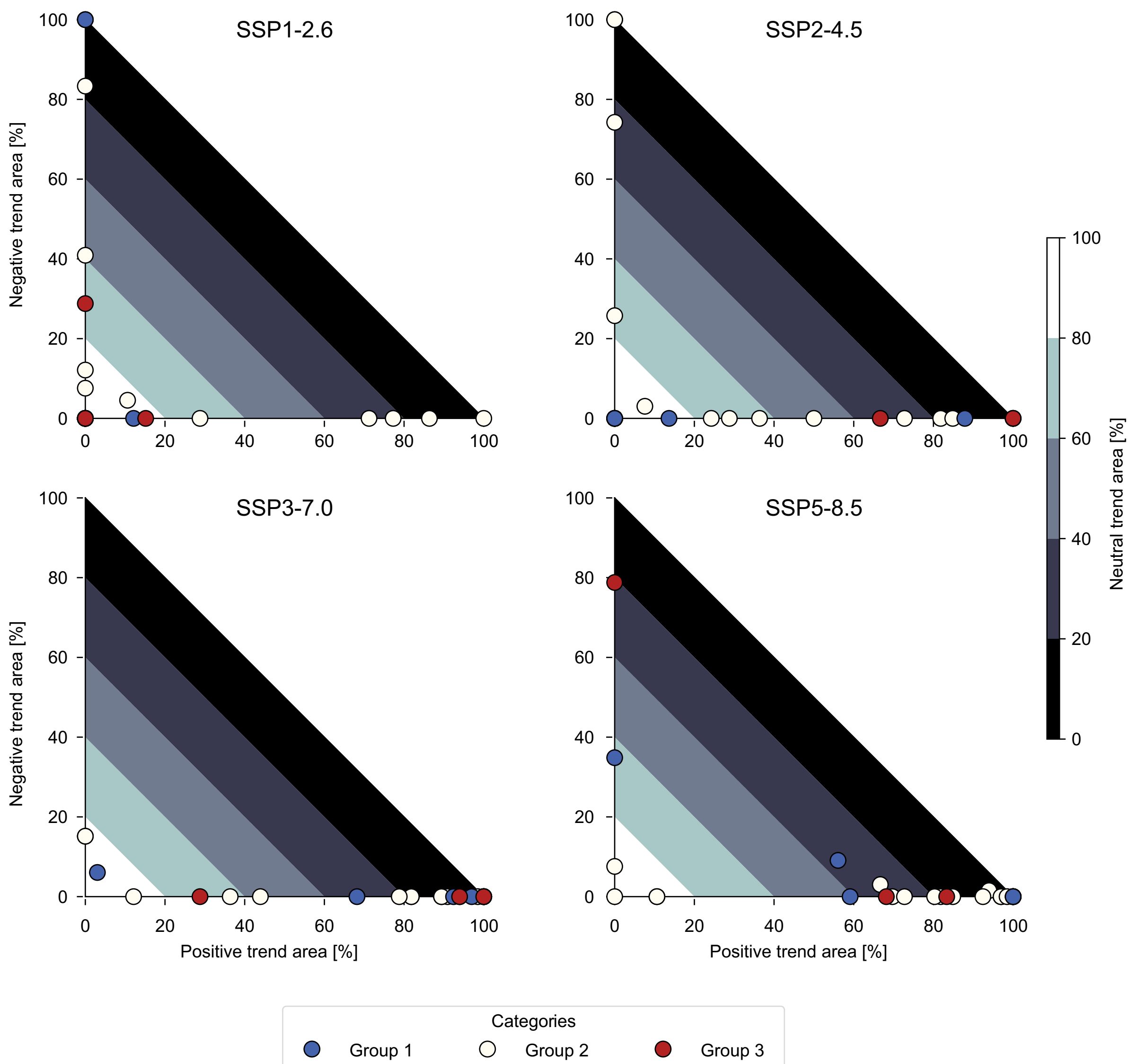

Fig. 12. Distribution diagrams of area percentage for trend categories of wind speed at 925 hPa in the CLLJ area, modeled by 34 CMIP6 models during the projection period, separated by climate change scenario. Group classifications are defined in section 3.2.

emission scenarios progressively increased the proportion of models projecting significant positive trends: SSP2-4.5 showed moderate strengthening, while SSP3-7.0 and SSP5-8.5 exhibited widespread intensification signals.

Ensemble mean time series revealed divergent trajectories after 2040. SSP1-2.6 maintained near-historical wind speeds, while SSP5-8.5 showed progressive strengthening reaching 0.8 m s^{-1} by 2099. The zonal component increasingly dominated, with easterly winds intensifying under high-emission scenarios, accompanied by enhanced northerly meridional flow, indicating trade-wind strengthening (Fig. 13).

Seasonal analysis uncovered pronounced asymmetry in projected changes. December-February showed weakening across all scenarios despite this being a current maximum period. June-August projections indicated strengthening proportional to emission levels. Most dramatically, September-November, currently the weakest season, showed

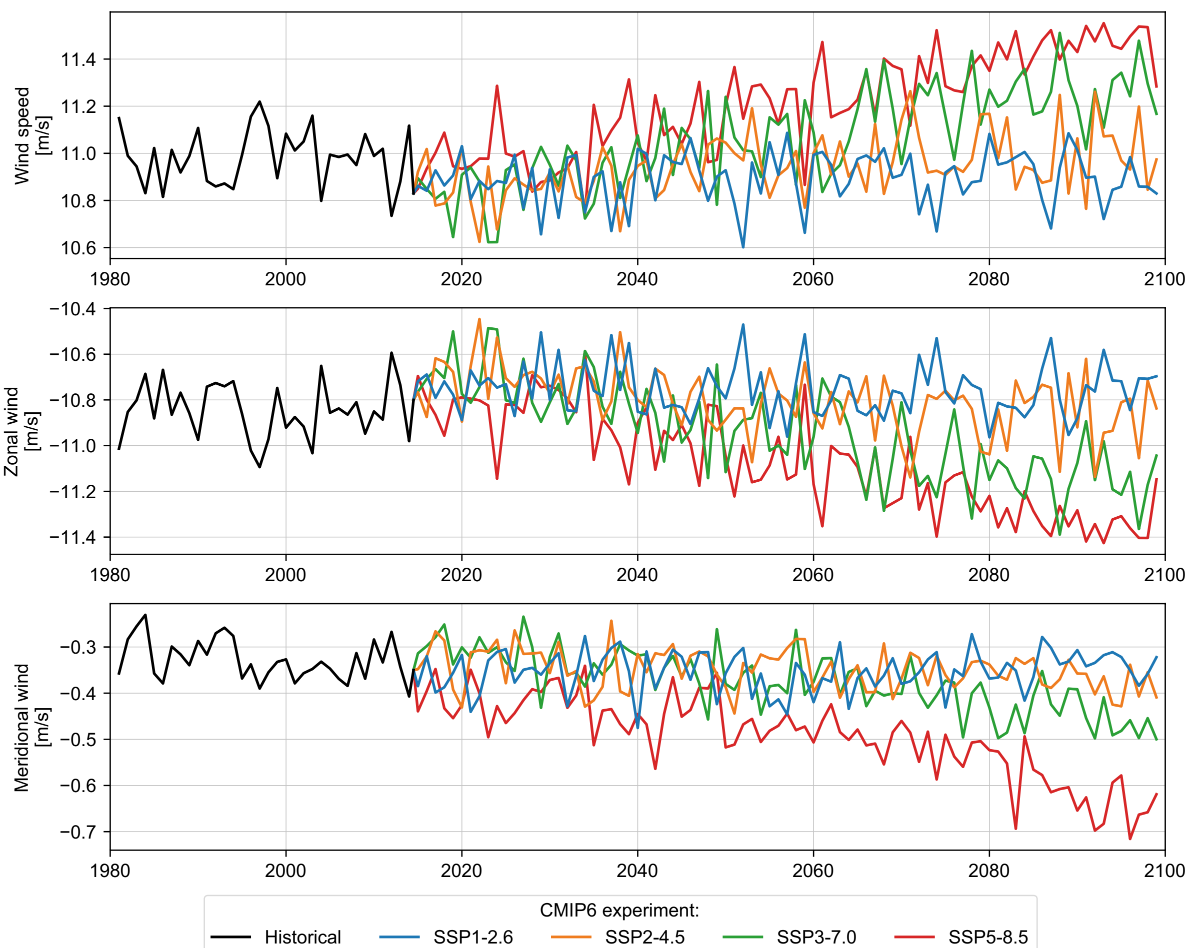

Fig. 13. Time series of ensemble mean wind speed and its components in the CLLJ area at 925 hPa for historical and projection periods under different scenarios.

maximum strengthening trends, potentially eliminating the current bimodal seasonal cycle under high-emission scenarios (Fig. 14).

Spatial patterns of ensemble-mean trends demonstrated coherent structures. Under SSP5-8.5, maximum strengthening concentrated in the CLLJ core region (12-16º N, 71-76º W), with trends exceeding 0.015 m s^{-1} y^{-1}. This intensification extended throughout the southern Caribbean basin, with implications for wind resources along Colombian coasts and moisture advection patterns across the region (Fig. 15).

Surface pressure trends provided a clear dynamical explanation for projected CLLJ changes. All scenario ensembles except SSP1-2.6 showed significant pressure increases over the NASH region, intensifying with emission levels. The Panama Low region exhibited weaker or non-significant pressure trends. This differential pressure evolution enhanced Caribbean pressure gradients in proportion to radiative forcing, thereby mechanistically explaining CLLJ strengthening under high-emission scenarios (Fig. 16).

Multi-model agreement on strengthening under strong forcing provides some robustness, particularly given the clear dynamical consistency with projected changes in pressure gradient. The enhanced moisture transport implied by stronger CLLJ could increase water vapor availability for precipitation along the Caribbean coasts of Central America, consistent with observed CLLJ-precipitation relationships (Whyte et al., 2007), while potentially reducing rainfall

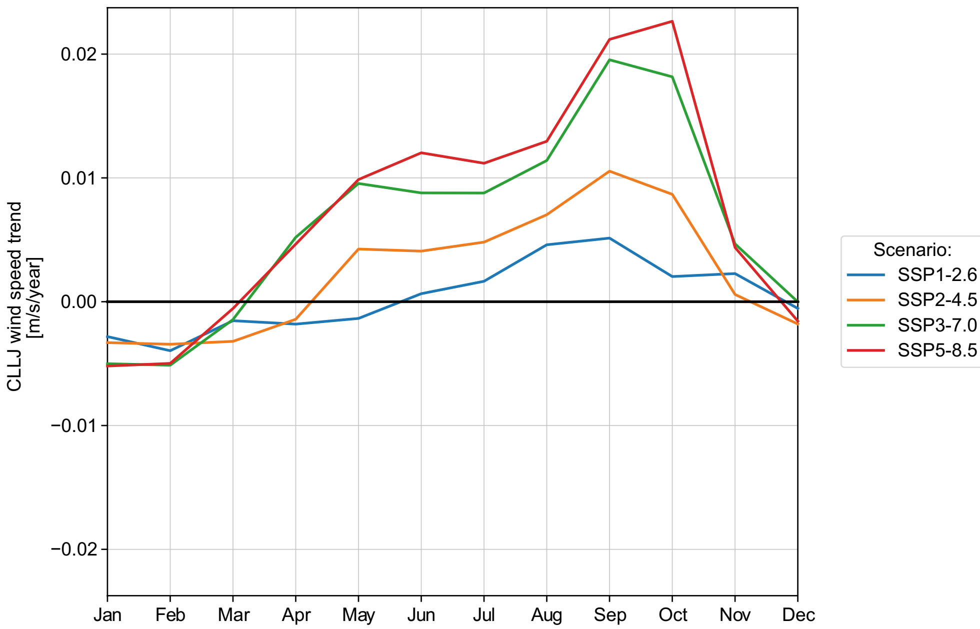

Fig. 14. Monthly trends of ensemble mean wind speed in the CLLJ area at 925 hPa during the projection period for each scenario.

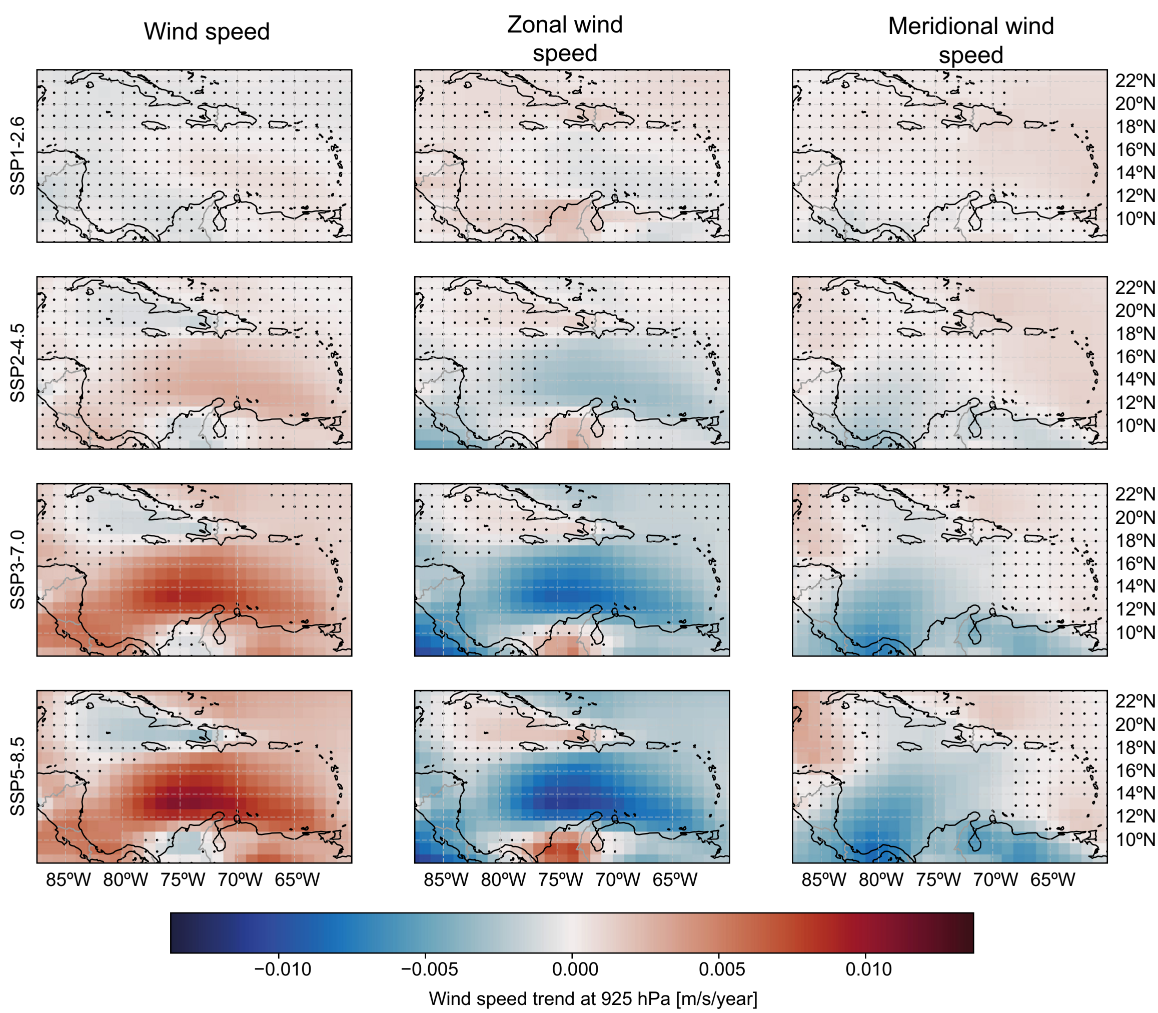

Fig. 15. Spatial distribution of wind speed trends at 925 hPa and its components from ensemble means by scenario during the projection period. Points indicate non-significant trends.

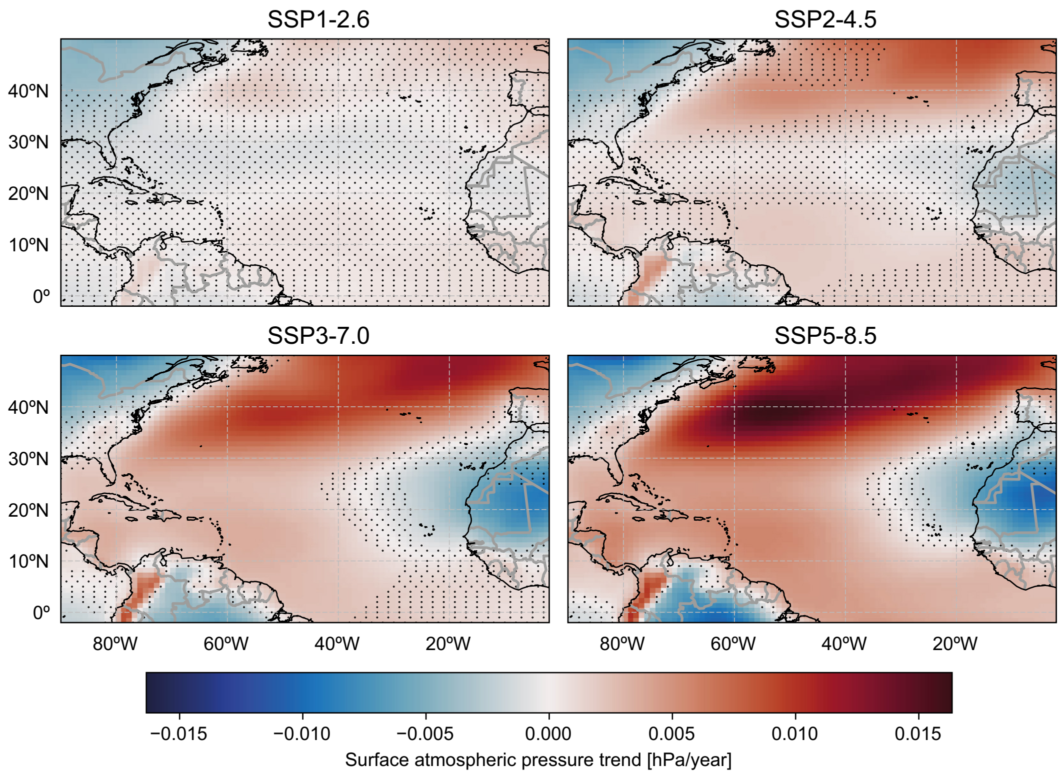

Fig. 16. Trend of surface atmospheric pressure from ensemble means by scenario during the projection period. Points indicate non-significant trends.

over Caribbean islands through enhanced moisture divergence.

The fundamental contradiction between historical observations and future projections raises critical questions about detection, attribution, and projection of regional wind changes. While multiple lines of evidence suggest recent weakening, CMIP6 models project strengthening under anthropogenic forcing. This discrepancy, combined with poor model performance during the historical period, introduces substantial uncertainty into future wind-resource and precipitation-pattern projections across the Caribbean region.

4. Conclusions

This comprehensive analysis of CLLJ changes reconciles conflicting historical evidence and projects scenario-dependent future evolution, with significant implications for regional moisture transport and precipitation. Key findings include:

Historical analysis (1981-2020) suggests CLLJ weakening, supported by three of four reanalyses (ERA5, MERRA-2, and 20th Century Reanalysis) showing –0.02 to –0.05 m s^{-1} y^{-1} trends at 925 hPa, dynamically consistent with pressure-gradient reductions between the NASH and Panama Low. Natural variability, driven by AMO/PDO modulation, likely contributed to the observed weakening, potentially masking any anthropogenic signal during this period.

CMIP6 models demonstrate limited skill in reproducing historical CLLJ characteristics, with only 24% achieving performance superior to climatological seasonal mean and 82% failing to capture observed weakening trends. These limitations, which echo biases documented in earlier CMIP generations by Martin and Schumacher (2011), extend to the representation of moisture transport and necessitate cautious interpretation of future projections.

Future projections show clear scenario dependence: SSP1-2.6 maintains current conditions; SSP2-4.5 shows moderate strengthening; and SSP3-7.0 and

SSP5-8.5 drive progressive strengthening through enhanced NASH intensification and Caribbean pressure gradients, with wind speeds increasing by up to 0.8 m s^{-1} by 2099 under the highest emission pathway. This strengthening implies enhanced moisture transport capacity with complex regional precipitation responses.

Seasonal changes redistribute CLLJ intensity and moisture transport, weakening winter maxima while strengthening autumn minima, potentially eliminating the current bimodal structure under high emissions and fundamentally altering precipitation patterns across Central America and northwestern South America.

These findings underscore the complex interplay between natural variability and anthropogenic forcing in shaping regional atmospheric circulation. The implications for regional water resources, agriculture, and renewable energy sectors are profound and require adaptive management strategies that account for projection uncertainties. Improved regional model representation, enhanced observational networks, and continued research on jet-precipitation relationships are essential for reducing uncertainties and informing adaptation strategies across the Caribbean region.

Future work should focus on dynamical downscaling to better resolve topographic influences on wind behavior and moisture transport, and on developing process-based metrics for evaluating model performance in simulating jet-hydroclimate interactions.

References

Amador JA. 2008. The Intra-Americas Sea low-level jet. Annals of the New York Academy of Sciences 1146: 153-188. https://doi.org/10.1196/annals.1446.012

Arregocés HA, Costa-Redondo LC, Rojano R. 2025. Exploring future projections of wind power density over the Caribbean region in CMIP6 models. Energy Reports 13: 3831-3844. https://doi.org/10.1016/j.egyr.2025.03.039

Bastidas-Salamanca M, Rueda-Bayona JG. 2021. Effect of climate variability events over the Colombian Caribbean offshore wind resource. Water 13: 3150. https://doi.org/10.3390/w13223150

Bustos Usta DF, Torres Parra RR. 2023. Projected wind changes in the Caribbean Sea based on CMIP6 models. Climate Dynamics 60: 3713-3727. https://doi.org/10.1007/s00382-022-06535-3

Cerón WL, Kayano MT, Andreoli RV, Ávila-Díaz A, de Souza IP, Souza RAF. 2021. Pacific and Atlantic multidecadal variability relations with the Choco and Caribbean low-level jets during the 1900-2015 period. Atmosphere 12: 1120. https://doi.org/10.3390/atmos12091120

Chen D, Rojas M, Samset BH, Cobb K, Diongue Niang A, Edwards P, Emori S, Faria SH, Hawkins E, Hope P, Huybrechts P, Meinshausen M, Mustafa SK, Plattner G-K, Tréguier A-M. 2021. Framing, Context, and Methods. In: Climate change 2021: The physical science basis (Masson-Delmotte V, Zhai P, Pirani A, Connors SL, Péan C, Berger S, Caud N, Chen Y, Goldfarb L, Gomis MI, Huang M, Leitzell K, Lonnoy E, Matthews JBR, Maycock TK, Waterfield T, Yelekçi O, Yu R, Zhou B, Eds.). Contribution of Working Group I to the Sixth Assessment Report of the Intergovernmental Panel on Climate Change. Cambridge University Press, Cambridge and New York, 147-286. https://doi.org/10.1017/9781009157896.003

Costoya X, de Castro M, Santos F, Sousa MC, Gómez-Gesteira M. 2019. Projections of wind energy resources in the Caribbean for the 21st century. Energy 178: 356-367. https://doi.org/10.1016/j.energy.2019.04.121

Durán-Quesada AM, Gimeno L, Amador J. 2017. Role of moisture transport for Central American precipitation. Earth System Dynamics 8: 147-161. https://doi.org/10.5194/esd-8-147-2017

Giannini A, Kushnir Y, Cane MA. 2001. Seasonality in the impact of ENSO and the North Atlantic High on Caribbean rainfall. Physics and Chemistry of the Earth, Part B: Hydrology, Oceans and Atmosphere 26: 143-147. https://doi.org/10.1016/S1464-1909(00)00231-8

Gil Ruiz SA, Cañón Barriga JE, Martínez JA. 2021. Wind power assessment in the Caribbean region of Colombia, using ten-minute wind observations and ERA5 data. Renewable Energy 172: 158-176. https://doi.org/10.1016/j.renene.2021.03.033

Gulev SK, Thorne PW, Ahn J, Dentener FJ, Domingues CM, Gerland S, Gong D, Kaufman DS, Nnamchi HC, Quaas J, Rivera JA, Sathyendranath S, Smith SL, Trewin B, von Schuckmann K, Vose RS. 2021. Changing State of the Climate System. In: Climate change 2021: The physical science basis (Masson-Delmotte V, Zhai P, Pirani A, Connors SL, Péan C, Berger S, Caud N, Chen Y, Goldfarb L, Gomis MI, Huang M, Leitzell

K, Lonnoy E, Matthews JBR, Maycock TK, Waterfield T, Yelekçi O, Yu R, Zhou B, Eds.). Contribution of Working Group I to the Sixth Assessment Report of the Intergovernmental Panel on Climate Change. Cambridge University Press, Cambridge and New York, 287-422. https://doi.org/10.1017/9781009157896.004

Herrera E, Magaña V, Caetano E. 2015. Air-sea interactions and dynamical processes associated with the midsummer drought. International Journal of Climatology 35: 1569-1578. https://doi.org/10.1002/joc.4077

Imbach P, Chou SC, Lyra A, Rodrigues D, Rodriguez D, Latinovic D, Siqueira G, Silva A, Garofolo L, Georgiou S. 2018. Future climate change scenarios in Central America at high spatial resolution. PLOS ONE 13: e0193570. https://doi.org/10.1371/journal.pone.0193570

Ma Y, Yuan N, Dong T, Dong W. 2023. On the Pacific Decadal Oscillation Simulations in CMIP6 models: A new test-bed from climate network analysis. Asia-Pacific Journal of Atmospheric Sciences 59: 17-28. https://doi.org/10.1007/s13143-022-00286-1

Martin ER, Schumacher C. 2011. The Caribbean Low-Level Jet and Its relationship with precipitation in IPCC AR4 models. Journal of Climate 24: 5935-5950. https://doi.org/10.1175/jcli-d-11-00134.1

Muñoz E, Busalacchi AJ, Nigam S, Ruiz-Barradas A. 2008. Winter and summer structure of the Caribbean Low-Level Jet. Journal of Climate 21: 1260-1276. https://doi.org/10.1175/2007JCLI1855.1

O'Neill BC, Tebaldi C, Van Vuuren DP, Eyring V, Friedlingstein P, Hurtt G, Knutti R, Kriegler E, Lamarque JF, Lowe J, Meehl GA, Moss R, Riahi K, Sanderson BM. 2016. The Scenario Model Intercomparison Project (ScenarioMIP) for CMIP6. Geoscientific Model Development 9: 3461-3482. https://doi.org/10.5194/gmd-9-3461-2016

Poveda G, Mesa OJ. 1999. La Corriente de Chorro Superficial del Oeste ("del CHOCÓ") y otras dos corrientes de chorro en Colombia: climatología y variabilidad durante las fases del ENSO. Revista de la Academia Colombiana de Ciencias Exactas Físicas y Naturales 23: 517-528.

Robson J, Sutton R, Menary MB, Lai MWK. 2023. Contrasting internally and externally generated Atlantic multidecadal variability and the role for AMOC in CMIP6 historical simulations. Philosophical Transactions of the Royal Society A: Mathematical, Physical and Engineering Sciences 381: 20220194. https://doi.org/10.1098/rsta.2022.0194

Taylor MA, Whyte FS, Stephenson TS, Campbell JD. 2012. Why dry? Investigating the future evolution of the Caribbean Low Level Jet to explain projected Caribbean drying. International Journal of Climatology 33: 784-792. https://doi.org/10.1002/joc.3461

Vichot-Llano A, Martínez-Castro D, Bezanilla-Morlot A, Centella-Artola A, Gil-Reyes L, Torres-Alavez JA, Corrales-Suástegui A, Giorgi F. 2022. Caribbean Low-Level Jet future projections using a multiparameter ensemble of RegCM4 configurations. International Journal of Climatology 42: 1544-1559. https://doi.org/10.1002/joc.7319

Wadoux AMJC, Walvoort DJJ, Brus DJ. 2022. An integrated approach for the evaluation of quantitative soil maps through Taylor and solar diagrams. Geoderma 405: 115332. https://doi.org/10.1016/j.geoderma.2021.115332

Wang C. 2007. Variability of the Caribbean Low-Level Jet and its relations to climate. Climate Dynamics 29: 411-422. https://doi.org/10.1007/s00382-007-0243-z

Whyte FS, Taylor MA, Stephenson TS, Campbell JD. 2007. Features of the Caribbean low level jet. International Journal of Climatology 28: 119-128. https://doi.org/10.1002/joc.1510

Supplementary material

Table SI. CMIP6 models used in this study.

Model name	Modeling center	Horizontal resolution (latitude × longitude)	Available experiments
ACCESS-CM2	Commonwealth Scientific and Industrial Research Organisation, Australian Research Council Centre of Excellence for Climate System Science	1.25º × 1.875º	Historical, SSP1-2.6, SSP2-4.5, SSP3-7.0, SSP5-8.5
AWI-CM-1-1-MR	Alfred Wegener Institute	0.935º × 0.938º	Historical, SSP1-2.6, SSP2-4.5, SSP3-7.0, SSP5-8.5
CanESM5-CanOE	Canadian Centre for Climate Modelling and Analysis	2.789º × 2.812º	Historical, SSP1-2.6, SSP2-4.5, SSP3-7.0, SSP5-8.5
CESM2	National Center for Atmospheric Research	0.942º × 1.25º	Historical, SSP1-2.6, SSP2-4.5, SSP3-7.0, SSP5-8.5
CESM2-WACCM	National Center for Atmospheric Research	0.942º × 1.25º	Historical, SSP3-7.0
CIESM	Tsinghua University Department of Earth System Science	0.942º × 1.25º	Historical, SSP1-2.6, SSP2-4.5, SSP5-8.5
CMCC-CM2-SR5	Centro Euro-Mediterraneo sui Cambiamenti Climatici	0.942º × 1.25º	Historical, SSP2-4.5, SSP3-7.0, SSP5-8.5
CMCC-ESM2	Centro Euro-Mediterraneo sui Cambiamenti Climatici	0.942º × 1.25º	Historical, SSP1-2.6, SSP2-4.5, SSP5-8.5
CNRM-CM6-1	National Center for Meteorological Research, Météo-France and CNRS laboratory, Climate Modeling and Global change	1.4º × 1.406º	Historical, SSP1-2.6, SSP2-4.5, SSP3-7.0, SSP5-8.5
CNRM-ESM2-1	National Center for Meteorological Research, Météo-France and CNRS laboratory, Climate Modeling and Global change	1.4º × 1.406º	Historical, SSP1-2.6, SSP2-4.5, SSP3-7.0, SSP5-8.5
EC-Earth3-AerChem	EC-Earth-Consortium	0.702º × 0.703º	Historical, SSP3-7.0
EC-Earth3-CC	EC-Earth-Consortium	0.702º × 0.703º	Historical, SSP2-4.5
EC-Earth3-Veg-LR	EC-Earth-Consortium	0.702º × 0.703º	Historical, SSP1-2.6, SSP2-4.5, SSP3-7.0, SSP5-8.5
FGOALS-f3-L	Chinese Academy of Sciences	1.0º × 1.25º	Historical, SSP1-2.6, SSP3-7.0, SSP5-8.5
FGOALS-g3	Chinese Academy of Sciences	2.621º × 2.0º	Historical, SSP1-2.6, SSP3-7.0, SSP5-8.5

Note: For models with heterogeneous horizontal resolution (non-uniform grid spacing), the average resolution is reported.

Table SI. CMIP6 models used in this study.

Model name	Modeling center	Horizontal resolution (latitude × longitude)	Available experiments
FIO-ESM-2-0	First Institute of Oceanography and Qingdao National Laboratory for Marine Science and Technology	0.942º × 1.25º	Historical, SSP1-2.6, SSP2-4.5, SSP5-8.5
GFDL-ESM4	National Oceanic and Atmospheric Administration, Geophysical Fluid Dynamics Laboratory	1.0º × 1.25º	Historical, SSP1-2.6, SSP2-4.5, SSP3-7.0, SSP5-8.5
HadGEM3-GC31-LL	Met Office Hadley Centre, Natural Environmental Research Council	1.25º × 1.875º	Historical, SSP1-2.6, SSP5-8.5
HadGEM3-GC31-MM	Met Office Hadley Centre	0.556º × 0.833º	Historical, SSP1-2.6, SSP5-8.5
INM-CM4-8	Institute of Numerical Mathematics	1.5º × 2.0º	Historical, SSP1-2.6, SSP2-4.5, SSP3-7.0, SSP5-8.5
INM-CM5-0	Institute of Numerical Mathematics	1.5º × 2.0º	Historical, SSP1-2.6, SSP2-4.5, SSP3-7.0, SSP5-8.5
IPSL-CM5A2-INCA	Institut Pierre-Simon Laplace	1.268º × 2.5º	Historical, SSP1-2.6, SSP3-7.0
IPSL-CM6A-LR	Institut Pierre-Simon Laplace	1.268º × 2.5º	Historical, SSP1-2.6, SSP2-4.5, SSP3-7.0, SSP5-8.5
KACE-1-0-G	National Institute of Meteorological Sciences, Korea Met. Administration	1.875º × 1.25º	Historical, SSP2-4.5, SSP3-7.0, SSP5-8.5
KIOST-ESM	Korea Institute of Ocean Science and Technology	1.875º × 1.875º	Historical, SSP1-2.6, SSP2-4.5, SSP5-8.5
MCM-UA-1-0	University of Arizona Department of Geosciences	2.235º × 3.75º	Historical, SSP1-2.6, SSP2-4.5, SSP3-7.0, SSP5-8.5
MIROC6	Atmosphere and Ocean Research Institute, Centre for Climate System Research National Institute for Environmental Studies	1.4º × 1.406º	Historical, SSP1-2.6, SSP2-4.5, SSP3-7.0, SSP5-8.5
MIROC-ES2L	Atmosphere and Ocean Research Institute, Centre for Climate System Research National Institute for Environmental Studies	2.789º × 2.812º	Historical, SSP1-2.6, SSP2-4.5, SSP3-7.0, SSP5-8.5
MPI-ESM1-2-LR	Max Planck Institute for Meteorology, Alfred Wegener Institute	1.865º × 1.875º	Historical, SSP1-2.6, SSP2-4.5, SSP3-7.0, SSP5-8.5
MRI-ESM2-0	Meteorological Research Institute, Japan	1.121º × 1.125º	Historical, SSP2-4.5, SSP3-7.0

Note: For models with heterogeneous horizontal resolution (non-uniform grid spacing), the average resolution is reported.

Table SI. CMIP6 models used in this study.

Model name	Modeling center	Horizontal resolution (latitude × longitude)	Available experiments
NESM3	Nanjing University of Information Science and Technology	1.864º × 1.875º	Historical, SSP1-2.6, SSP2-4.5, SSP5-8.5
NorESM2-MM	Norwegian Climate Centre	0.942º × 1.25º	Historical, SSP1-2.6, SSP2-4.5, SSP3-7.0, SSP5-8.5
TaiESM1	Research Center for Environmental Changes	0.942º × 1.25º	Historical, SSP1-2.6, SSP2-4.5, SSP3-7.0, SSP5-8.5
UKESM1-0-LL	Met Office Hadley Centre, Natural Environmental Research Council, National Institute of Meteorological Science / Korean Meteorological Administration, National Institute of Weather and Atmospheric Research	1.25º × 1.875º	Historical, SSP1-2.6, SSP2-4.5, SSP3-7.0, SSP5-8.5

Note: For models with heterogeneous horizontal resolution (non-uniform grid spacing), the average resolution is reported.